Available online at www.sciencedirect.com
ScienceDirect
Cement and Concrete Research 37 (2007) 109–117
Cement and Concrete Research

Composition and structure of C–S–H in white Portland cement–20% metakaolin pastes hydrated at 25 °C

C.A. Love [a], I.G. Richardson [a,*], A.R. Brough [a,b]

[a] School of Civil Engineering, University of Leeds, Leeds, LS2 9JT, United Kingdom
[b] Institute for Materials Research, University of Leeds, Leeds, LS2 9JT, United Kingdom

Received 16 July 2006; accepted 12 November 2006

Abstract

The microstructure and composition of water- and alkali-activated hardened pastes of white Portland cement–20% metakaolin blends have been studied using solid-state NMR spectroscopy and analytical TEM. The results show that after hydration for 1 day nearly half the cement had reacted in the water-activated paste but very little, if any, of the metakaolin; by 28 days two-thirds of the cement had reacted and most of the metakaolin. In contrast, whilst alkali-activation again led to about half the cement reacting by 1 day, about a quarter of the metakaolin had also reacted; and whilst most of the metakaolin had again reacted by 28 days, there had been no further reaction of the cement. The high degree of reaction of the MK in both pastes at 28 days resulted in long-chain highly aluminous C–S–H, with most of the bridging sites occupied by Al^{3+} rather than Si^{4+}. The data for the C–S–H in the water-activated paste are consistent with both the tobermorite/jennite (T/J) and tobermorite/calcium hydroxide (T/CH) models for the nanostructure of C–S–H – although very little J- or CH-like structure is needed to account for the observed compositions – whilst those for the alkali-activated paste can only be accounted for on the T/CH viewpoint.

Keywords: Metakaolin; NMR; TEM; C–S–H

1. Introduction

The reaction of metakaolin (MK) in blended cements has been studied quite extensively (for example [1–4]), mainly with the aim of characterizing the enhanced durability-related characteristics – such as chloride binding capacity [2] and refined pore structure [1] – that result from the replacement of cement with MK. Other studies have focused on the reaction of MK with calcium hydroxide [5,6], but the overall hydration products and microstructure that form in such systems are not the same as those formed with Portland cement. The aim of this study was to examine the hydration of a metakaolin–white Portland cement (WPC) blend when activated with either distilled water or 5 M KOH solution with a view to characterizing C–S–H that is highly substituted with aluminium. KOH solution was used to activate one of the pastes because the resulting C–S–H is structurally better ordered than that formed with water activation. This increased order results in narrower line widths in ^{29}Si NMR spectra. Individual peaks are consequently much better resolved, which makes deconvolution of the spectra relatively straightforward. The results from the KOH-activated pastes are then used to facilitate the deconvolution of those activated with water, as in previous work on blends involving blast-furnace slag [7]. Pastes were examined at 1 day and 28 days using solid-state ^{27}Al and ^{29}Si MAS NMR, and the results were compared to TEM–EDX analyses from pastes of the same composition hydrated for 28 days.

2. Experimental

Pastes of 20% MK–80% WPC were mixed at a liquid/solid ratio of 0.55 (ml/g) with either 5 M KOH solution or distilled water. Oxide analyses of the MK (Metastar 501 from Imerys) and WPC (Aalborg) are given in Table 1. The pastes were cast into 5-ml polypropylene vials and then individually heat sealed in plastic pouches and cured at 25 °C in a water bath until required.

* Corresponding author. Tel.: +44 113 343 2331; fax: +44 113 343 2265.
E-mail address: I.G.Richardson@leeds.ac.uk (I.G. Richardson).

0008-8846/$ - see front matter © 2006 Elsevier Ltd. All rights reserved.
doi:10.1016/j.cemconres.2006.11.012

Table 1
Bulk oxide composition for the white Portland cement and Metastar 501

Oxide (wt.%)	WPC	Metastar 501
SiO_2	25.00	52.00
TiO_2	0.08	0.03
Al_2O_3	2.14	37.33
Fe_2O_3	0.36	0.62
Mn_3O_4	0.02	0.01
MgO	0.78	0.27
CaO	71.02	0.07
Na_2O	<0.30	<0.30
K_2O	0.09	2.96
P_2O_5	0.08	0.10
Cr_2O_3	<0.01	<0.01
Total	99.57	93.41
LOI at 1025 °C	1.06	1.55

Solid-state single-pulse MAS NMR spectra were acquired using a Varian InfinityPlus 300 spectrometer (magnetic field 7.05 T; operating frequencies of 59.5 MHz for ^{29}Si and 78.2 MHz for ^{27}Al). Paste samples were freshly ground after 1 day and 28 days hydration. For the acquisition of ^{29}Si spectra, samples were packed into 6 mm zirconia rotors sealed at either end with Teflon end plugs, and spun at 6 kHz in a Chemagnetics-style probe. The spectra were acquired over 2400 scans using a pulse recycle delay of 5 s, a pulse width of 2 μs and an acquisition time of 20 ms; each spectrum therefore took about 200 min to acquire. For ^{27}Al, the samples were packed into 4 mm rotors sealed at either end with Teflon end caps and spun at 10 kHz in a 4 mm triple-resonance probe. This probe has a large aluminium probe background (one very large broad peak) so a background spectrum was acquired overnight and subtracted from the sample spectrum. The ^{27}Al spectra were acquired in the first hour of spinning to avoid dehydration and loss of intensity of peaks for AFt and AFm phases, which can occur with prolonged spinning [8,9]. The spectra were acquired over 6248 scans with a pulse recycle delay of 0.5 s, a pulse width of 1 μs and an acquisition time of 10 ms. Chemical shifts for aluminium are referenced to 1M $[Al(H_2O)_6]^{3+}$(aq) and silicon are referenced to TMS, using kaolinite as a secondary standard at −91.2 ppm.

Quantitative information on the fractions of Si present in silicate tetrahedra with different connectivities can be obtained from single-pulse ^{29}Si MAS NMR spectra. In this work, the spectra were fitted using a procedure that involves the subtraction of a contribution from a spectrum taken from anhydrous cement, which accounts for the unreacted alite and some of the belite, followed by the iterative fitting of the remaining belite and hydrate peaks to Voigt lineshapes using IgorPro [10]; a detailed description of the fitting procedure is given in [8]. The mean aluminosilicate chain length and the mean Al/Si ratio were calculated from the NMR data using Eqs. (1) and (2) in [11]. Fig. 1 shows an example of typical results of the deconvolution procedure for a KOH-activated paste; the figure includes – from top to bottom – the residual (×2), the experimental spectrum, and the fitted peaks. This last includes three peaks for the C–S–H: Q^1 (chain-end groups), Q^2 (middle-chain groups), and Q^2(1Al) (middle-chain groups where one of the adjacent tetrahedral sites is occupied by Al^{3+}), two for the remaining anhydrous WPC (Q^0) and one broad peak for the remaining MK (Q^4 type units).

Specimens for TEM were prepared from samples cured for 1 day and 28 days. Hydration was stopped using solvent

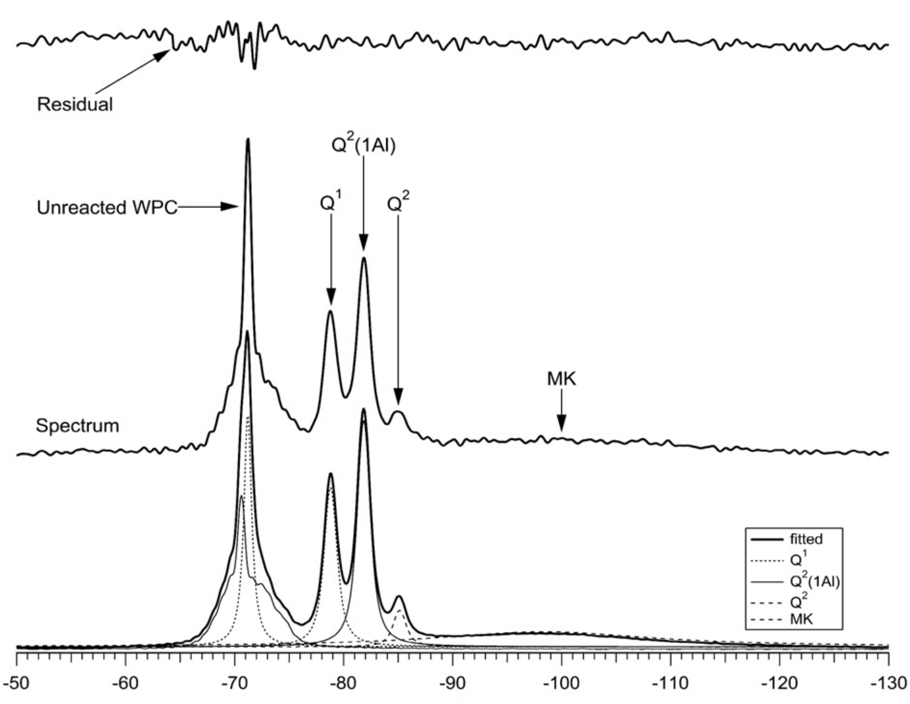

Fig. 1. Single-pulse ^{29}Si MAS NMR spectrum for a 5 M KOH-activated paste hydrated for 1 day (middle); the result of the deconvolution of the spectrum is shown at the bottom with the residual (×2) at the top. The hydrate peaks have chemical shifts of −78.8 ppm (Q^1), −81.8 ppm (Q^2(1Al)), and −85.1 ppm (Q^2(0Al)).

exchange with propan-2-ol. The sample preparation procedure for TEM is outlined in [12]. Samples for powder X-ray diffraction were freeze dried and ground. A Phillips APD 1700 diffractometer with Cu Kα radiation was used. Data were acquired from 5° to 65° 2θ with a scan speed of 0.025°/s and a step size of 0.05°.

3. Results

3.1. ^{27}Al NMR of pastes hydrated for 1 day and 28 days

Single-pulse ^{27}Al MAS NMR can distinguish between Al in different coordination states ($Al^{[4]}$, $Al^{[5]}$, and $Al^{[6]}$) in crystalline and poorly crystalline phases. Fig. 2 shows spectra for the anhydrous blend and pastes hydrated for 1 day and 28 days. In some cases the subtraction of the probe background has introduced small artefacts and a slight distortion of the baseline. Comparison of the spectra indicates that there are ten peaks in total (at 79, 70, 60, 56, 30, 28, 11, 8–9, 3, and 1 ppm). The assignment of the peaks is outlined in the following paragraphs.

The anhydrous metakaolin used in this study exhibits three main overlapping peaks with maxima at 56, 28 and around 1 ppm [8], which are indicated on the spectrum of the anhydrous blend at the bottom of Fig. 2. Following Skibsted et al. [13], the broad peak with a maximum at approximately 79 ppm on this spectrum is assigned to tetrahedrally coordinated Al in the WPC component. The spectra for the hydrated pastes of the KOH-activated blend show two main peaks, with maxima at around 70 ppm and around 8 ppm, which are assigned respectively to $Al^{[4]}$ in C–S–H and $Al^{[6]}$ in an AFm-type phase [14]. The spectrum for the 1-day KOH-activated paste also includes a peak at approximately 56 ppm for residual $Al^{[4]}$ in unreacted MK, which has disappeared by 28 days. There is an additional peak on the 28-day spectrum at approximately 60 ppm that is superimposed on the peak for $Al^{[4]}$ in C–S–H at 70 ppm; this peak is assigned to tetrahedral Al in an aluminosilicate anion in the interlayer of an AFm-type phase. This assignment is consistent with the chemical shift reported for $Al^{[4]}$ in strätlingite [15] and with the TEM–EDX data for an older specimen that showed the presence of Si in AFm crystals (a 4-year-old KOH-activated MK–WPC paste in which the AFm was sufficiently abundant to enable a large number of analyses to be collected [16]).

The spectra on Fig. 2 for the water-activated pastes also have peaks – assigned as above – with maxima at around 56 ppm (unreacted MK), and 9 ppm (an AFm-type phase). In addition, there is a sharp peak at 11 ppm, which is due to AFt, and a peak at around 3 ppm, which – following Andersen et al. [17] – is tentatively assigned to amorphous or poorly crystalline aluminium hydroxide gel or a calcium aluminate hydrate phase. A peak at around 60 ppm is present at 28 days and this is assigned, as above, to $Al^{[4]}$ in aluminosilicate anions in the interlayer of an AFm phase [15]. A minor peak at around 30 ppm that appears at 28 days – and must therefore be in a product rather than anhydrous material – is believed to be due to $Al^{[5]}$. Following Faucon et al. [18] – and supported by Andersen et al. [17,19] – this peak is tentatively assigned to Al substituting for Ca in the interlayer of C–S–H. A peak with this chemical shift and assigned to $Al^{[5]}$ was previously observed in a KOH-activated slag paste hydrated for 8 years [11] and is also observed in neat water-activated WPC pastes [8,17] and in water-activated PFA–WPC pastes [8].

Comparison of the spectra in Fig. 2 for the water-activated paste shows that between 1 and 28 days the peak for anhydrous

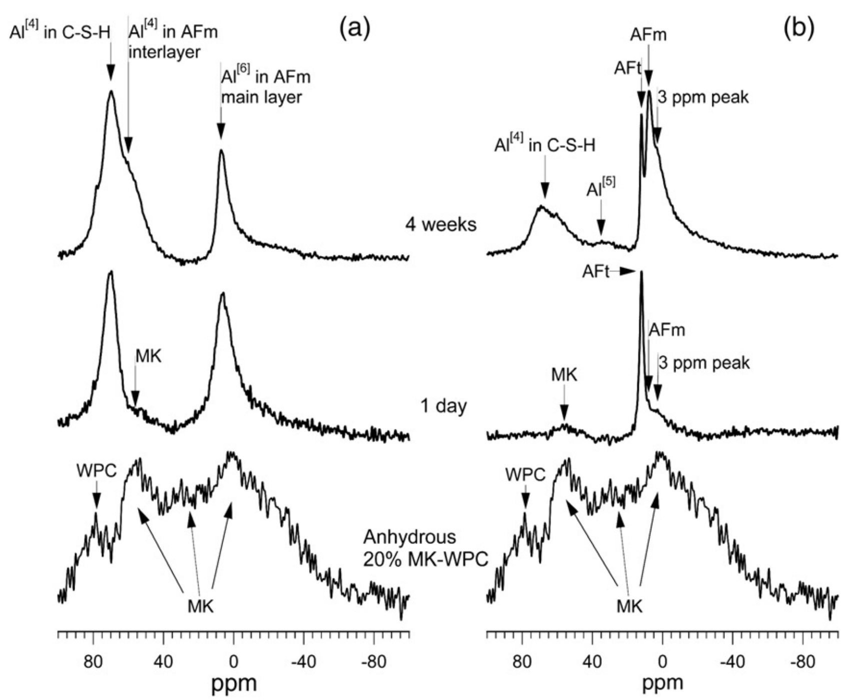

Fig. 2. Single-pulse ^{27}Al MAS NMR spectra (spun at 10 kHz) for the anhydrous blend (bottom), and KOH-activated (left) and water-activated (right) pastes hydrated for 1 (middle) and 28 days (top). All spectra are scaled to their tallest peak.

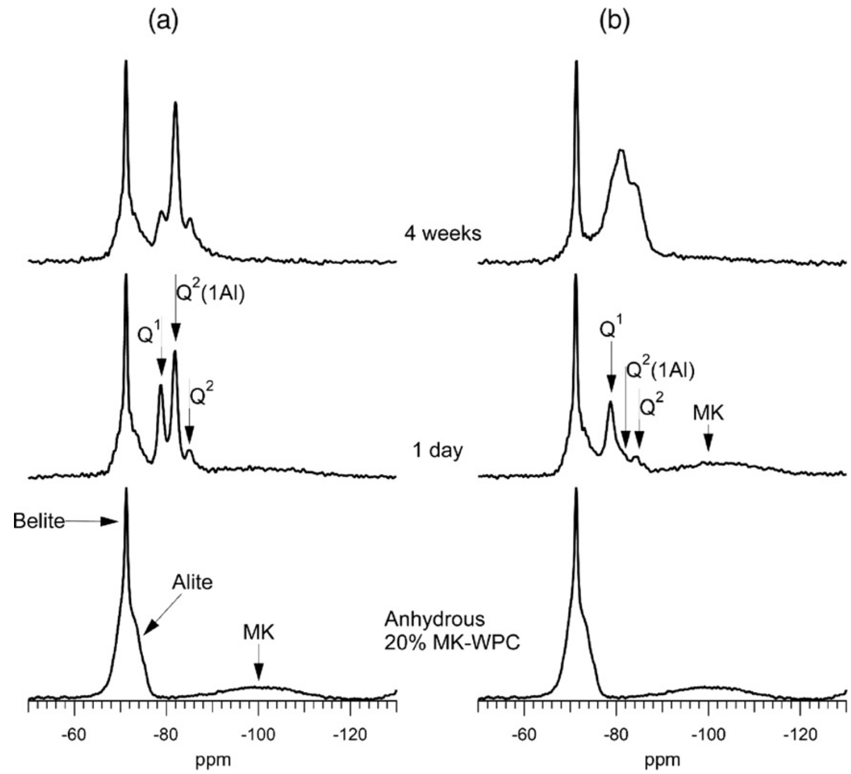

Fig. 3. Single-pulse ^{29}Si MAS NMR spectra (spun at 6 kHz) for the anhydrous blend (bottom), and KOH-activated (left) and water-activated (right) pastes hydrated for 1 (middle) and 28 days (top). All spectra are scaled to their tallest peak. The chemical shifts of the hydrate peaks (in ppm) in the order Q^1, Q^2(1Al), Q^2(0Al) are: −78.8, −81.8, −85.1 for 1 day–KOH; −78.8, −82.0, −85.5 for 28 days–KOH; −78.7, −81.3, −84.3 for 1 day–water; −78.8, −81.1, −84.4 for 28 days–water.

MK disappears, the amounts of AFt and AFm increase, and the peak for $Al^{[4]}$ present in C–S–H appears, as does the peak at around 30 ppm assigned to $Al^{[5]}$. This peak is not present in the KOH-activated spectra. In the KOH-activated pastes there is an increase in the amount of AFm and $Al^{[4]}$ in C–S–H between 1 day and 28 days, but more of the total Al is present in C–S–H and this becomes the tallest peak with increasing hydration. Both water and KOH-activated pastes seem to show some evidence by ^{27}Al NMR at 28 days of the formation of an AFm phase that contains an aluminosilicate anion (as in strätlingite) and so has an $Al^{[4]}$ as well as an $Al^{[6]}$ peak.

3.2. ^{29}Si NMR of pastes hydrated for 1 day and 28 days

Fig. 3 shows the single-pulse ^{29}Si NMR spectra for the anhydrous blend and for both the water- and KOH-activated pastes after 1 and 28 days hydration. Activation with KOH leads to better-resolved peaks for C–S–H indicating a higher degree of structural order. There is a large peak for Q^2(1Al) in the spectrum of the KOH-activated paste at 1 day, indicating the presence of long-chain Al-rich C–S–H, whereas the spectrum for the water-activated paste has Q^1 as the most intense hydrate peak, indicating that the C–S–H has shorter chains and is less Al substituted. The results from the deconvolution of the spectra are compared in Table 2. Whilst a quarter of the MK in the KOH-activated paste reacts by 1 day, there is essentially no reaction of the MK during this period in the water-activated paste. Both pastes, however, have about the same extent of WPC reaction, so the mean aluminosilicate chain length and the Al/Si ratio are consequently much higher at 1 day in the KOH-activated paste than in the water-activated.

Perhaps the most striking difference between the spectra at 1 and 28 days for the water-activated paste is a big increase in the Q^2(1Al) peak as hydration progresses, which is indicative of an increase in the mean aluminosilicate chain length and Al/Si ratio of the C–S–H (Table 2): as more cement and most of the MK react the chains polymerize and become more Al substituted. The Q^2(1Al) peak is still the largest hydrate peak in the KOH-activated paste at 28 days, but the Q^1 peak has decreased significantly and Q^2 increased slightly, resulting in an increase in mean aluminosilicate chain length and Al/Si ratio from 1 to 28 days (Table 2). The data in Table 2 confirm that most if not all the MK has reacted by 28 days (the lowest level detectible is estimated at around 10% of the initial Si present in the blend that

Table 2
Results from the deconvolution of the single-pulse ^{29}Si NMR spectra for water- and KOH-activated samples hydrated for 1 and 28 days

	% WPC reacted	% MK reacted	Al/Si	MCL	B (%)	B_{water}/B_{KOH} (%)
1 day water	46	0	0.06	2.8	55	61
1 day KOH	47	25	0.27	6.7	90	
28 days water	66	88	0.24	11.0	71	82
28 days KOH	39	100	0.34	15.7	87	

MCL = mean aluminosilicate chain length. B = bridging tetrahedra occupied by Al/bridging tetrahedra occupied by Al and Si.

was contributed by the MK). Unfortunately, microstructural inhomogeneities present in the KOH-activated paste caused by mixing problems are reflected in the NMR data (Table 2), which suggest that there is more unreacted cement left at 28 days than at 1 day, which is of course not possible.

3.3. Powder X-ray diffraction

Fig. 4 shows XRD traces for the Metastar 501 and both the KOH- and water-activated blends hydrated for 28 days. The trace for the Metastar 501 includes peaks for K-feldspar and mica superimposed on a broad hump for metakaolin, indicating that it contained a significant quantity of mineral impurities; the presence of these phases is consistent with the 3% K_2O detected by XRF (Table 1). Whilst peaks corresponding to the impurities can be identified on the traces for the pastes, they have clearly not been entirely inert, which is consistent with the results of Dow and Glasser [20]. The peaks for CH on the traces for the pastes are strikingly different in the two systems: water activation gives typical sharp well-defined peaks whereas KOH activation results in broad peaks, which is consistent with a small average crystal size. The C–S–H in the water-activated paste is nearly amorphous whilst in the KOH-activated system it has slightly more long-range structural order. In the KOH-activated paste the very broad peak at approximately 11.7° 2θ is due to an AFm phase, which is consistent with the NMR data. The absence of AFm peaks on the trace for the water-activated paste but presence of a peak assigned to AFm on the ^{27}Al NMR spectrum (Fig. 2) is a good illustration of the sensitivity of NMR

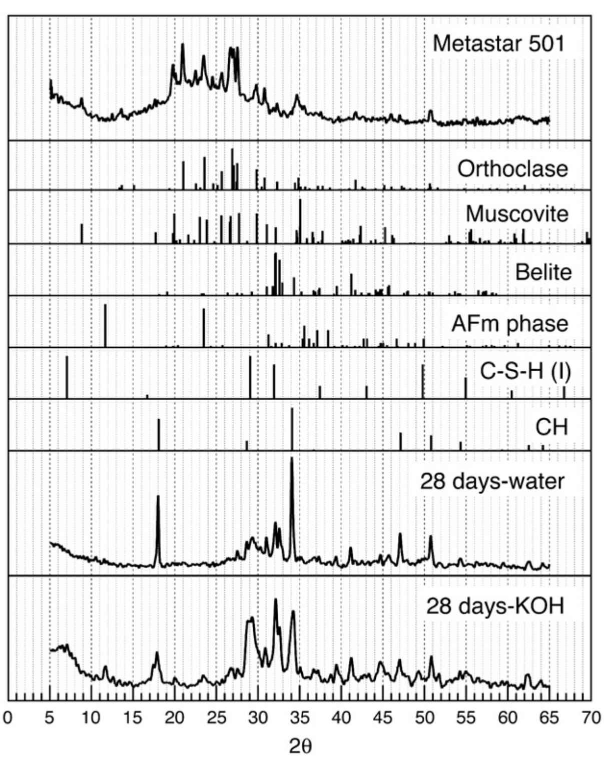

Fig. 4. XRD traces for the Metastar 501 and both the 28-day-old water- and KOH-activated pastes. Schematic X-ray powder diagrams are included for relevant phases.

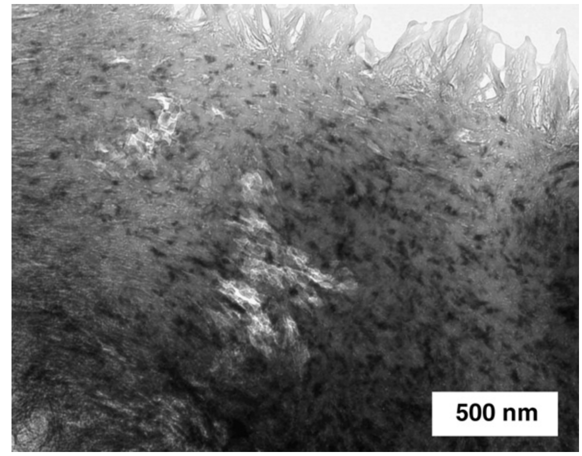

Fig. 5. A TEM micrograph from the KOH-activated paste hydrated for 1 day showing microcrystalline CH intermixed with Op C–S–H.

for detecting this phase – as noted previously [14] – which can be poorly ordered and present as very fine crystals (as observed by TEM, for example see [21]). Whilst the NMR data indicate that there is an AFm phase present in these systems that contains aluminosilicate anions in its interlayer, it is likely to be of variable composition with a number of different anions.

3.4. Transmission electron microscopy

Samples of both the KOH- and water-activated pastes were examined by TEM. The technique confirmed the microcrystalline nature of the CH in the KOH-activated system indicated by XRD; an example is shown in Fig. 5 where the CH microcrystals appear dark where they are oriented such that they Bragg-reflect electrons strongly. This is a typical feature of KOH-activated systems and has previously been observed in pastes of neat WPC activated with KOH, and in slag–WPC pastes activated with KOH [7]. Microcrystalline CH intermixed with C–S–H is not commonly observed in water-activated pastes, although examples have been reported, for example in pastes cured at elevated temperature [22] or of low water/

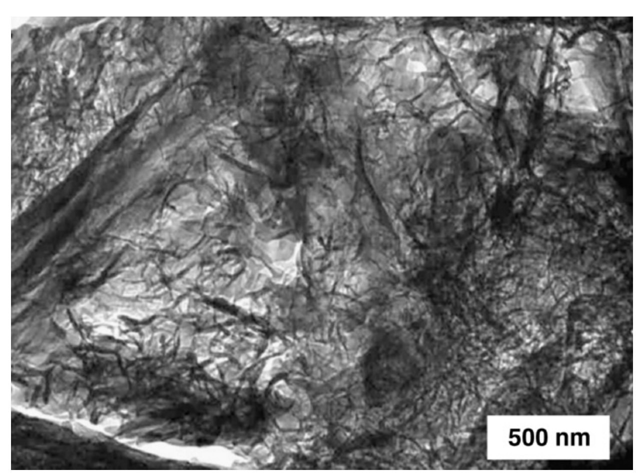

Fig. 6. A TEM micrograph from the KOH-activated paste hydrated for 28 days showing foil-like Op C–S–H and laths of AFm.

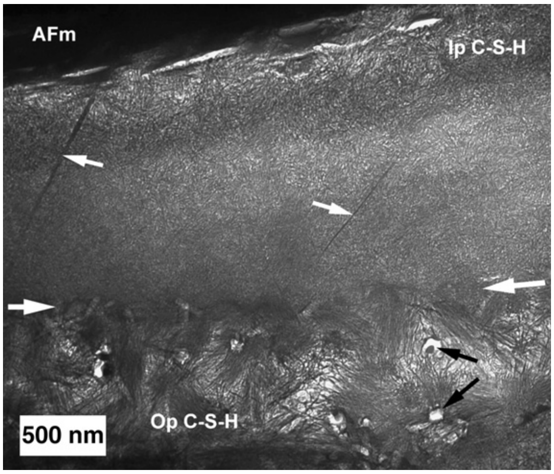

Fig. 7. A TEM micrograph from the water-activated paste hydrated for 28 days showing from bottom to top: relicts of AFt embedded in fine fibrillar Op C–S–H; very fine laths of AFm embedded in fine scale Ip C–S–H; a large crystal of AFm.

cement ratio [23]. Fig. 6 shows a typical micrograph from the KOH-activated paste at 28 days, showing that the outer product (Op) C–S–H has a foil-like morphology, and laths of an AFm type phase can also be seen (far left centre), intermixed with the

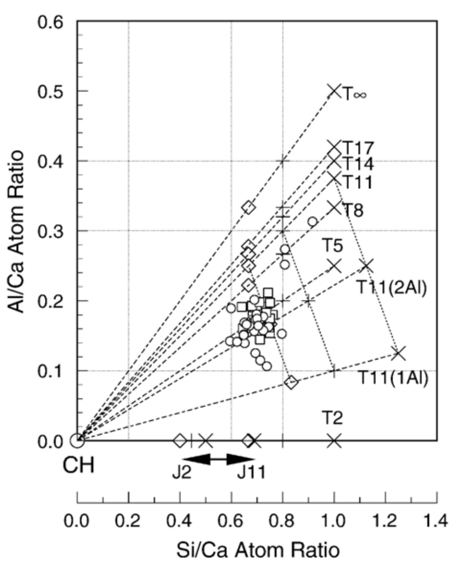

Fig. 8. Al/Ca against Si/Ca atom ratio plot of TEM–EDX analyses of Ip (□) and Op (○) C–S–H present in the water-activated paste hydrated for 28 days. The other symbols represent the compositions of tobermorite- (T) or jennite-based (J) structural units with different levels of protonation of the silicate chains: the minimum level (◊; $w/n=0$), an intermediate level (+; $w/n=1$), and the maximum level (×; $w/n=2$). Points are included on the figures that represent tobermorite-based units with chain lengths of 2, 5, 8, 11, 14, 17 and ∞. Most of the units are saturated with Al (i.e. all the occupied bridging sites are occupied by Al rather than Si). The only exceptions are units with 11 tetrahedra, which in addition to those saturated with Al (i.e. Al/(Al+Si)=3/11, which are labelled simply as T11), are also represented with one or two of the three bridging sites occupied by Al (i.e. Al/(Al+Si)=1/11 or 2/11): units with one or two Al ions are labelled as T11(1Al) and T11(2Al) respectively. T11 units with the same degree of protonation but different content of Al are joined by dotted lines. The dashed tie lines join points for structural units of the same length but different degrees of protonation with CH (at the origin).

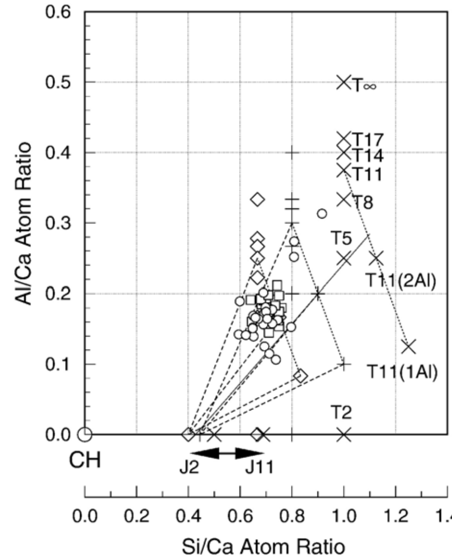

Fig. 9. As Fig. 8 except that the dashed tie lines now join points for T11 structural units with points on the Si/Ca axis that represent jennite-based dimer (with different degrees of protonation).

Op C–S–H. The Op C–S–H found in the water-activated paste has both fibrillar- and foil-like morphologies: a region with examples of both morphologies together with hexagonal-shaped relicts of AFt (examples indicated by small black arrows) is present in the bottom third of Fig. 7; for example, foil-like Op C–S–H is present directly below the white arrow that is near the right-hand edge of the micrograph. The central portion of the micrograph consists of very fine laths of AFm (indicated by small white arrows) embedded in inner product (Ip) C–S–H that has the typical, fine-scale morphology; the larger white arrows indicate the interface between the Ip and Op. The dark feature at the top of the micrograph is AFm.

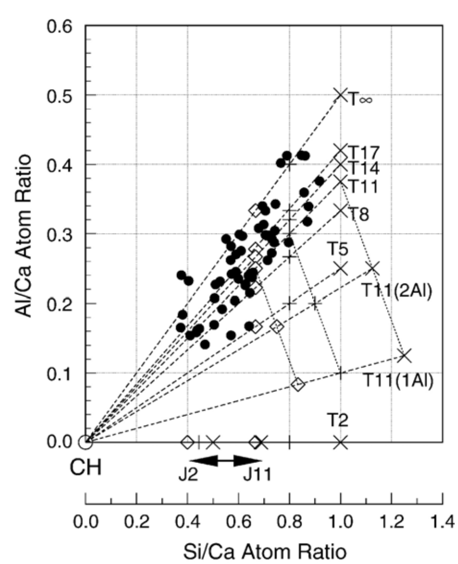

Fig. 10. As Fig. 8 except that the TEM–EDX data (●) are for Op C–S–H in the KOH-activated paste hydrated for 28 days. All analyzed regions (approx. 200 nm in diameter) were checked by selected area electron diffraction to be free of microcrystalline CH.

EDX analyses were taken from areas of C–S–H approximately 200 nm in size. The areas were first checked by selected area electron diffraction to be free of crystalline phases. Analyses for the water-activated paste at 28 days are plotted in Figs. 8 and 9, and analyses for the KOH-activated paste are plotted in Fig. 10. The mean Ca/Si ratio of the C–S–H in the water-activated paste is 1.43 (standard deviation, S.D. = 0.11; n = 50), the mean Al/Si ratio is 0.25 (S.D. = 0.04; n = 50) and the mean Ca/(Si + Al) ratio is 1.14 (S.D. = 0.09; n = 50), whilst in the KOH-activated paste the corresponding values are 1.67 (S.D. = 0.41; n = 56), 0.42 (S.D. = 0.07; n = 56), and 1.18 (S.D. = 0.28; n = 56). The data for the KOH-activated sample are for Op C–S–H only since no areas of Ip C–S–H were found that were sufficiently large to analyze. The TEM data together with the mean aluminosilicate chain length and the degree of occupation of bridging sites by Al (calculated from the deconvoluted fits of the ^{29}Si NMR spectra according to the equations given in [22]) are considered in the Discussion section in terms of the two main nanostructural viewpoints for C–S–H; that is, either tobermorite–jennite or tobermorite–CH models ([22], and references therein).

4. Discussion

The C–S–H that is formed by the reaction of the 20% MK–WPC blend with water is mainly dimeric at 1 day, with a mean aluminosilicate chain length of 2.8. In contrast, the C–S–H in the KOH-activated paste at the same age has a mean aluminosilicate chain length of 6.7. 46% of the WPC had reacted by 1 day in the water-activated paste and very little, if any, of the MK. The same amount of WPC had reacted in the KOH-activated paste (47%) but much more of the MK (25%), indicating that activation with KOH rather than water accelerates the MK reaction, which leads to the rapid formation of aluminous long-chain C–S–H. AFt is produced with water activation, but not with KOH. After 28 days, both pastes show an increase in mean aluminosilicate chain length and Al/Si ratio, consistent with the reaction of most of the MK in both pastes. At this age, Al^{3+} ions occupy approximately 70% of the bridging sites in the C–S–H in the water-activated paste (mean aluminosilicate chain length of 11), and approximately 90% in the KOH-activated paste (mean aluminosilicate chain length of 16). Interestingly, similar increases in the degree of Al substitution between water- and alkali-activated pastes have been observed previously for slag–WPC blends [7].

Small relicts of AFt and both very fine laths and quite large crystals of AFm were observed in the water-activated paste by TEM (Fig. 7). This is consistent with the ^{27}Al NMR spectra, which include peaks assigned to these phases, although they were not detected by XRD. Laths of an AFm-type phase were also observed by TEM of the KOH-activated paste (Fig. 6), which is again consistent with presence of an $Al^{[6]}$ peak (with a peak maximum at around 8 ppm) in the ^{27}Al NMR spectra (Fig. 2). However, AFt was not observed in the TEM or detected by NMR, indicating that it does not form in the presence of high levels of alkali. Since microcrystalline CH forms in the KOH-activated paste, it is reasonable to suppose that some of the AFm in this system may also occur at a similarly fine scale.

There is excellent agreement at 28 days between the bulk Al/Si ratio of the C–S–H calculated from the NMR data and the value determined directly by TEM (of both Ip and Op C–S–H) for the water-activated paste (0.24 and 0.25, respectively). The agreement is less good for the KOH-activated paste (0.34 by NMR and 0.42 by TEM), but this may be due in part to a lack of TEM analyses of Ip C–S–H, together with the inherent variability of the samples for this system due to the mixing problems (i.e. the lack of analyses of Ip C–S–H was quite possibly a sample preparation/sampling issue). Also, the positions of a number of points on Fig. 10 indicate that perhaps some of the Op analyses contain a contribution from AFm intermixed with C–S–H on a scale < 200 nm (in particular, those points that lie above the line T∞–CH).

4.1. Discussion of the data in terms of models for the nanostructure of C–S–H

Figs. 8–10 include TEM–EDX analyses of C–S–H present in the pastes, and also points that represent various structural units in Richardson and Groves' model for the nanostructure of C–S–H that has substituent ions [22,25]. The model includes formulations that are based on structural elements derived from tobermorite intermixed with others derived from either jennite (the T/J viewpoint) or calcium hydroxide (the T/CH viewpoint): an explanation of the different symbols and tie lines on the figures is given in the Appendix. Fig. 8 includes the TEM–EDX data for the water-activated paste hydrated for 28 days (both Op (○) and Ip C–S–H (□)). Each data point corresponds to an analysis of C–S–H that had been checked by selected area electron diffraction to not be intermixed with a crystalline phase. The mean aluminosilicate chain length for the C–S–H in this paste was 11, with 71% of the occupied bridging sites occupied by Al; that is, an average structural unit would have 11 tetrahedra with Al^{3+} ions at two of the three bridging sites and Si^{4+} at the third. Consideration of the positions of the EDX data points with those of the structural units, and with the tie lines between the units and the origin, clearly shows that the C–S–H in this system can be accounted for on the T/CH structural viewpoint. The same TEM–EDX data are shown on Fig. 9, but in this case the dashed lines join T11 units that have varying degrees of protonation and Al content, with J2 units, which also have varying degrees of protonation. The TEM–EDX data points again fall between the dashed lines, this time indicating that the data can be accounted for on the T/J viewpoint, but only if some of the J-like structure contains short chains (e.g. a number of the points would be outside the model if only J11 units were considered). Since the TEM–NMR data are consistent with both structural viewpoints, it is evident that additional information is needed to decide which is most appropriate (or, indeed, a mixture of the two), although it is also apparent that very little J- or CH-like structure is necessary to account for the observed compositions (with a low mean Ca/(Si + Al) ratio of 1.14), if there is a low degree of protonation of the aluminosilicate chains, which is well demonstrated by formulae (1) and (2), which represent average structural units with minimum and maximum degrees of protonation respectively (on the T/CH viewpoint and with the assumption that the substitution of Si^{4+} by Al^{3+} is balanced entirely by Ca^{2+} ions):

$$Ca_{12.58}H_{1.03}(Si_{0.8}Al_{0.2})_{11}O_{34}\cdot mH_2O \tag{1}$$

$$Ca_{9.1}H_8(Si_{0.8}Al_{0.2})_{11}O_{34}\cdot 3.48Ca(OH)_2\cdot mH_2O \tag{2}$$

A significant level of T-based structure would be consistent with the observation that much of the Op C–S–H has foil-like morphology; if the observed fibrillar morphology were taken to be due to the presence of jennite-like structure, then those structural units would clearly need to have a degree of protonation above the minimum. TEM–EDX data for C–S–H in the KOH-activated system are presented on Fig. 10. In this case the mean aluminosilicate chain length was about 16, with around 90% of the occupied bridging sites occupied by Al; that is, an average structural unit would be long-chain with almost all its bridging sites occupied by Al^{3+} ions rather than Si^{4+}. On inspection, it is clear that, in contrast to the water-activated paste, the data can only be accounted for on the T/CH viewpoint; the T/J viewpoint cannot account for the data. The association of T-based structure with Op C–S–H (in the KOH-activated system) that has foil-like morphology is in agreement with results for other systems [22]. The narrow distribution of chemical analyses and presence of fibrillar Op C–S–H morphology in the water-activated system is also consistent with results for other systems [22].

5. Conclusions

The microstructure and composition of water- and alkali-activated hardened pastes of white Portland cement–20% metakaolin blends have been studied using solid-state ^{29}Si and ^{27}Al MAS NMR spectroscopy and analytical TEM. The results show that after hydration for 1 day nearly half the cement had reacted in the water-activated paste but very little, if any, of the metakaolin; by 28 days two-thirds of the cement had reacted and most of the metakaolin. In contrast, whilst alkali-activation again led to about half the cement reacting by 1 day, about a quarter of the metakaolin had also reacted; and whilst most of the metakaolin had again reacted by 28 days, there had been no further reaction of the cement. The high degree of reaction of the MK in both pastes at 28 days resulted in long-chain highly aluminous C–S–H, with most of the bridging sites occupied by Al^{3+} rather than Si^{4+}. The TEM–NMR data for the C–S–H in the water-activated paste are consistent with both T/J and T/CH models for the nanostructure of C–S–H – although very little J- or CH-like structure is needed to account for the observed compositions – whilst those for the alkali-activated paste can only be accounted for on the T/CH viewpoint. The outer product C–S–H has both fine-fibrillar and foil-like morphologies in the water-activated paste and a crumpled foil-like morphology in the KOH-activated paste. The results are consistent with foil-like morphology being associated with T-based structure, which is in agreement with results for other systems [21].

Acknowledgements

Thanks are due to the Engineering and Physical Sciences Research Council for funding under Grant Nos. GR/S45874/01 and GR/R07073/01 and for a PhD studentship (CAL), to a number of industrial collaborators for additional financial and technical support (UK Nirex, Castle Cement, Lafarge, and W.R. Grace), and to an anonymous reviewer for comments that resulted in improvements in the manuscript.

Appendix A

Structural units from Richardson and Groves' model for the nanostructure of Al-substituted C–S–H are represented on Figs. 8–10 with three different symbols, which correspond to different degrees of protonation of the silicate chains: the minimum (◊, $w/n=0$ in Formula (14) of [24]), an intermediate level (+, $w/n=1$), and the maximum (×, $w/n=2$). For the purpose of straightforward illustration, in all cases it is assumed that the substitution of Al^{3+} for Si^{4+} ions is balanced by monovalent alkali cations; charge compensation by 0.5 Ca^{2+} would of course slightly alter the position of the units (see Figs. 2 and 3 in [25], the Discussion in [7], and Eq. (13) in [22]). Al^{3+} is assumed to only substitute for Si^{4+} in tobermorite-based units and not in jennite-based (this is discussed in [25]). Points are included on the figures that represent tobermorite-based units with chain lengths of 2, 5, 8, 11, 14, 17 and ∞. Most of the units are saturated with Al (i.e. all the occupied bridging sites are occupied by Al rather than Si). The only exceptions are units with 11 tetrahedra, which in addition to those saturated with Al (i.e. $Al/(Al+Si)=3/11$, which are labelled simply as T11), are also represented with one or two of the three bridging sites occupied by Al (i.e. $Al/(Al+Si)=1/11$ or 2/11): units with one or two Al ions are labelled as T11(1Al) and T11(2Al), respectively. T11 units with the same degree of protonation but different content of Al are joined by dotted lines; the Si/Ca ratio decreases and Al/Ca ratio increases linearly as the number of bridging sites that are occupied by Al and not Si increases. For a given degree of protonation of the silicate chains the T units that are saturated with Al all have the same Si/Ca ratio, regardless of the chain length: they differ only in Al/Ca ratio, which increases with increasing chain length. So, for example, dimeric units with the maximum possible degree of protonation have Si/Ca = 1 and Al/Ca = 0 (because dimeric units have no bridging tetrahedra). The longer chains that have this degree of protonation have the same Si/Ca ratio but Al/Ca ratios that increase with increasing chain length up to a maximum of 0.5 for infinitely long chains; that is, they occur on Fig. 8 vertically above the point for the T2 unit. Decreasing the degree of protonation results in a linear reduction in the Al/Ca and Si/Ca ratios; on Fig. 8 points that represent units with the same chain length and Al/Si ratio but which have different degrees of protonation are joined by dashed lines (which when extended intersect at the origin). On the T/CH viewpoint, the dashed lines between the origin and the units with the minimum degree of protonation (◊) represent T units intermixed with layers of CH; regions between the units with minimum (◊) and maximum (×) degree of protonation represent either a variation in the degree of protonation or an intermixture of units that have a high level of protonation with layers of CH. Since Al^{3+} is assumed not to substitute for Si^{4+} in jennite-based units and since any Al in octahedral co-ordination is assumed to occur in layers of AFm-type structure (see [25] for a discussion of this), the J units all have zero Al/Ca and so occur along the Si/Ca axis. Only four J units are represented on Fig. 8: the point at Si/Ca = 0.4 represents J2 units with the minimum degree of protonation (◊, $J2^{w/n=0}$ in Formula (14) of [24]), the two points immediately to the right of this are also J2 units but with intermediate (+, $J2^{w/n=1}$) and maximum (×, $J2^{w/n=2}$) levels of protonation, and the point at Si/Ca = 0.68 represents J11 units with maximum degree of protonation (×, $J11^{w/n=2}$). The double-headed arrow indicates the range of composition possible for J units with chain length between 2 and 11. The point between $J2^{w/n=2}$ and $J11^{w/n=2}$ is $T2^{w/n=2}$ (with Si/Ca = 0.667).

References

[1] P. Bredy, M. Chabannet, J. Pera, Microstructure and porosity of metakaolin blended cements, Mater. Res. Soc. Symp. Proc. 136 (1989) 275–280.

[2] N.J. Coleman, C.L. Page, Aspects of the pore solution chemistry of hydrated cement pastes containing metakaolin, Cem. Concr. Res. 2 (1997) 147–154.

[3] A.M. Dunster, J.R.M. Parsonage, M.J.K. Thomas, The pozzolanic reaction of metakaolinite and its effects on Portland cement hydration, J. Mater. Sci. 28 (1993) 1345–1350.

[4] B.B. Sabir, S. Wild, J. Bai, Metakaolin and calcined clays as pozzolans for concrete: a review, Cem. Concr. Compos. 23 (2001) 441–454.

[5] J.G. Cabrera, M. Frías Rojas, Mechanism of hydration of the metakaolin–lime–water system, Cem. Concr. Res. 31 (2001) 177–182.

[6] P.S. DeSilva, F.P. Glasser, Phase relations in the system $CaO–Al_2O_3–SiO_2–H_2O$ relevant to metakaolin–calcium hydroxide hydration, Cem. Concr. Res. 23 (1993) 627–639.

[7] I.G. Richardson, G.W. Groves, The structure of the calcium silicate hydrate phases present in hardened pastes of white Portland cement/blast-furnace slag blends, J. Mater. Sci. 32 (1997) 4793–4802.

[8] C.A. Love, Ph.D. Thesis, University of Leeds, (2002).

[9] J.A. Chudek, G. Hunter, M.R. Jones, S.N. Scrimgeour, P.C. Hewlett, A.B. Kudryavtsev, Aluminium-27 solid state NMR spectroscopic studies of chloride binding in Portland cement and blends, J. Mater. Sci. 35 (2000) 4275–4288.

[10] IgorPro, Wavemetrics Inc., Lake Oswego, OR 97035, USA.

[11] I.G. Richardson, A.R. Brough, G.W. Groves, C.M. Dobson, The characterization of hardened alkali-activated blast-furnace slag pastes and the nature of the calcium silicate hydrate (C–S–H) phase, Cem. Concr. Res. 24 (5) (1994) 813–829.

[12] I.G. Richardson, Electron microscopy of cements, in: P. Barnes, J. Bensted (Eds.), Chapter 22 in Structure and Performance of Cements, 2nd ed., Spon Press, London, 2002, pp. 500–556.

[13] J. Skibsted, H.J. Jacobsen, C. Hall, Direct observation of aluminium guest ions in the silicate phases of cement minerals by ^{27}Al MAS NMR spectroscopy, J. Chem. Soc., Faraday Trans. 90 (14) (1994) 2095–2098.

[14] J. Skibsted, E. Henderson, H.J. Jakobsen, Characterization of calcium aluminate phases in cements by ^{27}Al MAS NMR spectroscopy, Inorg. Chem. 32 (1993) 1013–1027.

[15] W. Geβner, D. Müller, Festkörper–NMR–untersuchungen am gehlenite-hydrat $2CaO·Al_2O_3·8H_2O$, Zeit. Chem. 29 (1989) 344–345.

[16] Unpublished data.

[17] M.D. Andersen, H.J. Jakobsen, J. Skibsted, Incorporation of aluminium in the calcium silicate hydrate (C–S–H) of hydrated Portland cements: a high field ^{27}Al and ^{29}Si MAS NMR investigation, Inorg. Chem. 42 (2003) 2280–2287.

[18] P. Faucon, A. Delgrave, J.C. Petit, C. Richet, J.M. Marchand, H. Zanni, Aluminium incorporation in calcium silicate hydrates (C–S–H) depending on their Ca/Si ratio, J. Phys. Chem., B 103 (1999) 7796–7802.

[19] M.D. Andersen, H.J. Jakobsen, J. Skibsted, A new aluminium–hydrate species in hydrated Portland cements characterized by ^{27}Al and ^{29}Si MAS NMR spectroscopy, Cem. Concr. Res. 36 (2006) 3–17.

[20] C. Dow, F.P. Glasser, Alkali releases from crushed minerals and thermally activated constituents of metakaolin, Adv. Cem. Res. 15 (2003) 137–143.

[21] I.G. Richardson, G.W. Groves, Microstructure and microanalysis of hardened ordinary Portland cement pastes, J. Mater. Sci. 28 (1993) 265–277.

[22] I.G. Richardson, Tobermorite/jennite and tobermorite/calcium hydroxide-based models for the structure of C–S–H: applicability to hardened pastes of tricalcium silicate, β-dicalcium silicate, Portland cement, and blends of Portland cement with blast-furnace slag, metakaolin or silica fume, Cem. Concr. Res. 34 (2004) 1733–1777.

[23] G.W. Groves, Microcrystalline calcium hydroxide in Portland-cement pastes of low water–cement ratio, Cem. Concr. Res. 11 (1981) 713–718.

[24] I.G. Richardson, G.W. Groves, Models for the composition and structure of calcium silicate hydrate (C–S–H) gel in hardened tricalcium silicate pastes, Cem. Concr. Res. 22 (1992) 1001–1010.

[25] I.G. Richardson, G.W. Groves, The incorporation of minor and trace elements into calcium silicate hydrate (C–S–H) gel in hardened cement pastes, Cem. Concr. Res. 23 (1993) 131–138.